Engineering Analysis with Boundary Elements 36 (2012) 779–788

Contents lists available at SciVerse ScienceDirect

Engineering Analysis with Boundary Elements

journal homepage: www.elsevier.com/locate/enganabound

A fast multipole boundary element method for 3D multi-domain acoustic scattering problems based on the Burton–Miller formulation

Haijun Wu [a], Yijun Liu [b], Weikang Jiang [a,*]

[a] State Key Laboratory of Machinery System and Vibration, Shanghai Jiao Tong University, Shanghai 200240, China
[b] Mechanical Engineering, University of Cincinnati, Cincinnati, OH 45221-0072, USA

ARTICLE INFO

Article history:
Received 9 August 2011
Accepted 30 November 2011

Keywords:
Boundary element method
Fast multipole method
Acoustics
Multi-domain
Multi-layered
Effective moment computations

ABSTRACT

A fast multipole boundary element method (FMBEM) for 3D multi-domain acoustic scattering problems based on the Burton–Miller formulation is presented in this paper. A multi-tree structure is designed for the multi-domain FMBEM. It results in mismatch of leaves and well separate cells definition in different domains and complicates the implementation of the algorithm, especially for preconditioning. A preconditioner based on boundary blocks is devised for the multi-domain FMBEM and its efficiency in reducing the number of iterations in solving large-scale multi-domain scattering problems is demonstrated. In addition to the analytical moment, another method, based on the anti-symmetry of the moment kernel, is developed to reduce the moment computation further by a factor of two. Frequency sweep analysis of a penetrable sphere shows that the multi-domain FMBEM based on the Burton–Miller formulation can overcome the non-unique solution problem at the fictitious eigenfrequencies. Several other numerical examples are presented to demonstrate the accuracy and efficiency of the developed multi-domain FMBEM for acoustic problems. In spite of the high cost of memory and CPU time for the multi-tree structure in the multi-domain FMBEM, a large BEM model studied with a PC has 0.3 million elements corresponding to 0.6 million unknowns, which clearly shows the potential of the developed FMBEM in solving large-scale multi-domain acoustics problems.

1. Introduction

Fast multipole method (FMM), one of the top ten algorithms of the last century, was first innovated by Rokhlin and Greengard [1–3] in the mid of 1980s. In conjunction with iterative equation solvers (GMRES [4], CG [5], etc.), FMM can reduce the matrix vector multiplication dramatically, as well as the memory requirement to $O(N^a \log N^b)$, where $1 \leq a < 2$ and $b \geq 0$ in solving boundary element method (BEM) equation systems, with N being the number of elements. These advantages overcome the well-known drawbacks with regard to the computational efficiency and memory requirement of the conventional BEM and make the fast multipole BEM (FMBEM) one of the most popular fast solution methods for the BEM.

Initially, the FMBEM was developed and implemented for the potential problems such as N-body dynamics and the Dirichlet problem based on the Laplace equation [1–3]. Recently, acoustic problems have been solved by the FMBEM widely. Sakuma and Yasuda [6,7] developed a FMBEM for the large-scale steady-state sound field analysis. Gumerov and Duraiswami [8] presented a fast multipole method to compute the scattering from clusters of spheres. The FMBEM for solving structural–acoustic interaction problems was developed by Fisher, Gauland Brunner et al. [9–11]. Adaptive algorithms for the FMBEM were developed to speed up the solutions for 3-D full- and half-space acoustic problems by Shen, Bapat and Liu [12–14]. Analytical expressions of the moments in the diagonal FMBEM, which can further speed up the solutions, were derived [15], and is applied to the multi-domain FMBEM in this paper. The FMBEM used in Refs. [6–10,12–15] can be divided into two groups, one is named low frequency FMBEM and another is called high frequency FMBEM. Both of them will be inefficient or fail out of their preferred frequency range. To overcome the numerical instabilities of the low and high frequency FMBEM, several wide-band FMBEM have been developed recently. Darve and Havé [16] proposed a stable-plane-wave expansion, which has a lower computational cost than the multipole expansion and does not have the accuracy and stability problems of the plane-wave expansion. Two hybrid FMBEM were developed by Cheng et al. [17], Gumerov and Duraiswami [18], which are stable for a wide range of frequencies. The former switches to different representations at low and high frequencies, while the latter is based on a rotation–coaxial translation–back rotation scheme. More information about the fast multipole BEM in general can be found in a review article [19], and the first textbook [20].

* Corresponding author. Tel.: +86 21 34206332 824; fax: +86 21 34205783.
E-mail address: wkjiang@sjtu.edu.cn (W. Jiang).

0955-7997/$ - see front matter © 2011 Elsevier Ltd. All rights reserved.
doi:10.1016/j.enganabound.2011.11.018

In the field of acoustics, studies have been devoted mostly to the single domain FMBEM even though the multi-domain or multi-layered BEM had been used to analyze acoustic problems using the conventional BEM. Cheng et al. [21] used the multi-domain BEM to analyze the muffler problems. An excellent agreement with the finite element solution was observed in the transmission loss prediction for different muffler configurations. Sarradj [22] presented a multi-domain BEM for the calculation of sound fields in and around porous absorbers having a rigid frame. Seydou [23] developed a boundary integral equation approach for solving the multi-layered acoustic problems in a three dimensional space and validated the algorithm by comparing the approximated results with the exact results. Coupled structural acoustics has also been done by Chen and Liu [24] using the BEM. To the author's best knowledge, the FMBEM based on the Burton–Miller formulation has not been applied to solve 3D multi-domain acoustic problems.

In the multi-domain acoustic problems, new challenges appear to the FMBEM due to the less favorable conditioning of the systems of BEM equations caused by medium parameter mismatch between adjacent domains, thin domains, etc. The use of preconditioners [25–27] can significantly improve the convergence rates in the FMBEM iterative solution. In this paper, different from the usual FMBEM, each domain is assigned a tree structure in the multi-domain FMBEM. Different cell definitions among trees complicate the multi-domain FMBEM implementation and its preconditioning. A boundary block diagonal preconditioner which is based on a single closed boundary division, not a leaf in a domain tree structure, is devised to reduce the number of iterations.

The remaining part of the paper is organized as follows. An overview of the boundary integral formulation for the multi-domain acoustic problems is provided in Section 2. A brief introduction of the FMM and the FMBEM based on the Burton–Miller formulation for the multi-domain acoustic problems are given in Section 3. Moreover, an effective moment computation based on the anti-symmetric moment kernel, multi-tree structure and a preconditioner based on the boundary blocks are also introduced in the Section 3. Several numerical examples are studied up to verify the accuracy, efficiency and applicability of the developed FMBEM for solving large-scale multi-domain acoustic problems in Section 4. Section 5 concludes this paper and presents some discussions concerning the multi-domain FMBEM.

2. BIE formulation for 3D multi-domain acoustic problems

We consider the acoustic wave scattering problem in an infinite domain E_{L+1} with an obstacle E_L that contains other acoustic sub-domains. Let E_l, $l=1,2,\ldots,L+1$ be $L+1$ domains divided by L boundaries S_l, $l=1,2,\ldots,L$, shown in Fig. 1. In the lth domain, the sound speed and mass density are c_l and $\overline{\rho}_l$, respectively, the wavenumber is defined by $k_l=\omega/c_l$ (also called circular or angular wavenumber in some references), in which ω is the angular frequency of the incident wave. The normal direction of the boundary of each domain is also indicated in Fig. 1.

As shown in Fig. 1, every boundary or interface belongs to two neighboring domains. Due to continuity conditions, sound pressure φ are equal on each boundary S_λ. So that, it is easy to get the pressure boundary condition, for boundary S_λ

$$\varphi_{li}(\boldsymbol{y})=\varphi_{lo}(\boldsymbol{y})=\varphi_\lambda(\boldsymbol{y}) \quad \text{for } \boldsymbol{y}\in S_\lambda, \tag{1}$$

in which li and lo are numbers of the two domains which share the same boundary S_λ, and the two domains are named inner domain and outer domain of the boundary S_λ. Another boundary condition is derived from the continuous velocity condition and

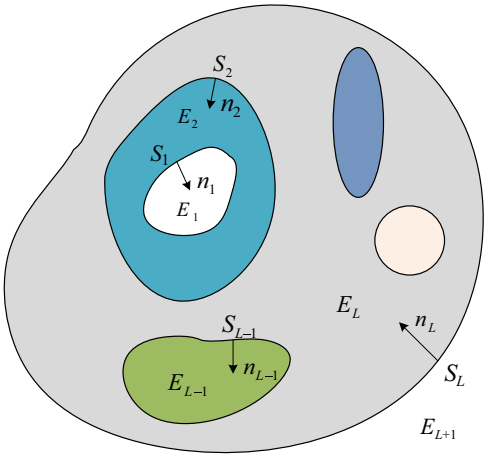

Fig. 1. A multi-domain model.

Euler's equation. It states

$$\frac{\partial\varphi_{li}(\boldsymbol{y})}{\partial n_\lambda(\boldsymbol{y})}=\frac{\overline{\rho}_{li}}{\overline{\rho}_{lo}}\frac{\partial\varphi_{lo}(\boldsymbol{y})}{\partial n_\lambda(\boldsymbol{y})}. \tag{2}$$

Define

$$q_\lambda^l(\boldsymbol{y})=\frac{\partial\varphi_l(\boldsymbol{y})}{\partial n_\lambda(\boldsymbol{y})}, \tag{3}$$

where $q_\lambda^l(\boldsymbol{y})$ means the normal gradient of sound pressure by letting $\boldsymbol{y}$ approach to the boundary S_λ from the domain E_l side.

The velocity boundary condition can be rewritten as

$$q_\lambda^{li}=\rho_\lambda q_\lambda \quad \text{for } \lambda=1,\ldots,L, \tag{4}$$

in which $\rho_\lambda=\overline{\rho}_{li}/\overline{\rho}_{lo}$ and $q_\lambda=q_\lambda^{lo}$.

Suppose Γ_l is the boundary set of the domain E_l and boundaries in domain Γ_l are smooth, as shown in Fig. 1, boundary set Γ_1 contains only boundary S_1, boundary set Γ_2 contains boundaries S_1 and S_2, boundary set Γ_L composes of boundaries S_l with l being $2,\ldots,L$, and boundary set Γ_{L+1} contains boundary S_L. Therefore, the conventional boundary integral equation (CBIE) in each domain is

$$\frac{1}{2}\varphi_\lambda(\boldsymbol{x})=\sum_{S_\tau\subset\Gamma_l}\int_{S_\tau}\left[G_l(\boldsymbol{x},\boldsymbol{y})q_\tau^l(\boldsymbol{y})-\varepsilon_\tau^l\frac{\partial G_l(\boldsymbol{x},\boldsymbol{y})}{\partial n_\tau(\boldsymbol{y})}\varphi_\tau(\boldsymbol{y})\right]dS(\boldsymbol{y}) + \varphi^I(\boldsymbol{x}) \quad \text{for } \boldsymbol{x}\in S_\lambda\backslash\Gamma_l, \tag{5}$$

in which $l=1,\ldots,L+1$, ε_τ^l is the normal direction coefficient of boundary S_τ for domain E_l, $\varepsilon_\tau^l=-1$ if $l=\tau$ and $\varepsilon_\tau^l=1$ if $l>\tau$, $\varphi^I(\boldsymbol{x})$ is the incident wave and presents just in the outermost domain for scattering problems. In this paper, the time convention adopted is $e^{-i\omega t}$, correspondingly, the free-space Green's function for 3-D problems in the lth domain is

$$G_l(\boldsymbol{x},\boldsymbol{y})=\frac{e^{ik_lr}}{4\pi r} \quad \text{with } r=|\boldsymbol{x}-\boldsymbol{y}| \tag{6}$$

Non-uniqueness of the CBIE solution in exterior acoustic problems solution appears when the frequency of the incident wave coincides with the corresponding interior problems' eigenfrequency. To deal with the non-uniqueness difficulties, Burton and Miller [28] proposed a method by combining the CBIE and the normal derivative of the CBIE. Taking the derivative of the integral representation with respect to the normal at the field point $\boldsymbol{x}$ leads to the following hyper-singular boundary integral equation (HBIE):

$$\frac{1}{2}q_\lambda^l(\boldsymbol{x})=\sum_{S_\tau\subset\Gamma_l}\int_{S_\tau}\left[\frac{\partial G_l(\boldsymbol{x},\boldsymbol{y})}{\partial n_\lambda(\boldsymbol{x})}q_\tau^l(\boldsymbol{y})-\varepsilon_\tau^l\frac{\partial^2 G_l(\boldsymbol{x},\boldsymbol{y})}{\partial n_\lambda(\boldsymbol{x})\partial n_\tau(\boldsymbol{y})}\varphi_\tau(\boldsymbol{y})\right]dS(\boldsymbol{y}) + \frac{\partial\varphi^I(\boldsymbol{x})}{\partial n_\lambda(\boldsymbol{x})} \quad \text{for } \boldsymbol{x}\in S_\lambda\backslash\Gamma_l, \tag{7}$$

in which $l=1,\ldots,L+1$. Define operators as

$$\mathcal{S}^{\lambda}_{l,\tau}q^l_\tau(\boldsymbol{y})=\int_{S_\tau}G_l(\boldsymbol{x},\boldsymbol{y})q^l_\tau(\boldsymbol{y})dS(\boldsymbol{y}) \text{ for } \boldsymbol{x}\in S_\lambda\backslash\Gamma_l, \tag{8}$$

$$\mathcal{D}^{\lambda}_{l,\tau}\varphi_\tau(\boldsymbol{y})=\varepsilon^l_\tau\int_{S_\tau}\frac{\partial G_l(\boldsymbol{x},\boldsymbol{y})}{\partial n_\tau(\boldsymbol{y})}\varphi_\tau(\boldsymbol{y})\,dS(\boldsymbol{y}) \text{ for } \boldsymbol{x}\in S_\lambda\backslash\Gamma_l, \tag{9}$$

$$\mathcal{M}^{\lambda}_{l,\tau}q^l_\tau(\boldsymbol{y})=\int_{S_\tau}\frac{\partial G_l(\boldsymbol{x},\boldsymbol{y})}{\partial n_\tau(\boldsymbol{x})}q^l_\tau(\boldsymbol{y})\,dS(\boldsymbol{y}) \text{ for } \boldsymbol{x}\in S_\lambda\backslash\Gamma_l, \tag{10}$$

$$\mathcal{H}^{\lambda}_{l,\tau}\varphi_\tau(\boldsymbol{y})=\varepsilon^l_\tau\int_{S_\tau}\frac{\partial^2 G_l(\boldsymbol{x},\boldsymbol{y})}{\partial n_\lambda(\boldsymbol{x})\partial n_\tau(\boldsymbol{y})}\varphi_\tau(\boldsymbol{y})\,dS(\boldsymbol{y}) \text{ for } \boldsymbol{x}\in S_\lambda\backslash\Gamma_l. \tag{11}$$

A linear combination of Eqs. (5) and (7) yields the following well-known Burton–Miller formulation (CHBIE or dual BIE) which has unique solutions at all frequencies:

$$\sum_{S_\tau\backslash\Gamma_l}\{[\mathcal{D}^{\lambda}_{l,\tau}+\beta_l\mathcal{H}^{\lambda}_{l,\tau}]\varphi_\tau(\boldsymbol{y})-[\mathcal{S}^{\lambda}_{l,\tau}+\beta_l\mathcal{M}^{\lambda}_{l,\tau}]q^l_\tau(\boldsymbol{y})\}$$
$$+\frac{1}{2}[\varphi_\lambda(\boldsymbol{x})+\beta_l q^l_\lambda(\boldsymbol{x})]=\varphi^I(\boldsymbol{x})+\beta_l\frac{\partial\varphi^I(\boldsymbol{x})}{\partial n_\lambda(\boldsymbol{x})} \text{ for } \boldsymbol{x}\in S_\lambda\backslash\Gamma_l, \tag{12}$$

in which $l=1,\ldots,L+1$, β_l is a coupling constant that must be a complex number and can be chosen, for example, as i/k_l. Taking the boundary conditions into account, for the multi-domain acoustic problems, there are actually $2L$ sets of unknown quantities defined on the L boundaries which will lead to $2L$ set of BIE equations. Those BIE equations can be ordered according to domains or to boundaries. Due to the mismatch of mediums in different domains, the discretized BIE equations can have very poor condition numbers which are not favorable in solutions with iterative solvers. Therefore, the BIE equations should be ordered into a form which permits easy preconditioning and hence can reduce the number of iterations. As suggested in Ref. [29], the discretized form of the multi-domain BEM equations can be ordered according to boundaries as follows:

$$\begin{bmatrix}
\boldsymbol{A}^1_{1,1} & \rho_1\boldsymbol{B}^1_{1,1} & \boldsymbol{0} & \boldsymbol{0} & \cdots & \boldsymbol{0} & \boldsymbol{0}\\
\boldsymbol{A}^1_{2,1} & \boldsymbol{B}^1_{2,1} & \boldsymbol{A}^1_{2,2} & \rho_2\boldsymbol{B}^1_{2,2} & \cdots & \boldsymbol{0} & \boldsymbol{0}\\
\boldsymbol{A}^2_{2,1} & \boldsymbol{A}^2_{2,1} & \boldsymbol{A}^2_{2,2} & \rho_2\boldsymbol{B}^2_{2,2} & \cdots & \boldsymbol{0} & \boldsymbol{0}\\
\boldsymbol{0} & \boldsymbol{0} & \boldsymbol{A}^2_{L,2} & \boldsymbol{B}^2_{L,2} & \cdots & \boldsymbol{A}^2_{L,L} & \rho_L\boldsymbol{B}^2_{L,L}\\
\vdots & \vdots & \vdots & \vdots & \ddots & \vdots & \vdots\\
\boldsymbol{0} & \boldsymbol{0} & \boldsymbol{0} & \boldsymbol{0} & \cdots & \boldsymbol{A}^L_{L,L} & \rho_L\boldsymbol{B}^L_{L,L}\\
\boldsymbol{0} & \boldsymbol{0} & \boldsymbol{0} & \boldsymbol{0} & \cdots & \boldsymbol{A}^L_{L+1,L} & \boldsymbol{B}^L_{L+1,L}
\end{bmatrix}
\begin{bmatrix}\boldsymbol{\varphi}_1\\ \boldsymbol{q}_1\\ \boldsymbol{\varphi}_2\\ \boldsymbol{q}_2\\ \vdots\\ \boldsymbol{\varphi}_L\\ \boldsymbol{q}_L\end{bmatrix}=
\begin{bmatrix}\boldsymbol{0}\\ \boldsymbol{0}\\ \boldsymbol{0}\\ \boldsymbol{0}\\ \vdots\\ \boldsymbol{0}\\ \boldsymbol{b}_L\end{bmatrix}, \tag{13}$$

in which $\boldsymbol{A}^{\lambda}_{l,\tau}$ and $\boldsymbol{B}^{\lambda}_{l,\tau}$ are sub-matrices defined as

$$\boldsymbol{A}^{\lambda}_{l,\tau}=\frac{1}{2}\delta_{\lambda,\tau}\boldsymbol{I}+\mathcal{D}^{\lambda}_{l,\tau}+\beta_l\mathcal{H}^{\lambda}_{l,\tau}, \tag{14}$$

$$\boldsymbol{B}^{\lambda}_{l,\tau}=\frac{\beta_l}{2}\delta_{\lambda,\tau}\boldsymbol{I}-(\mathcal{S}^{\lambda}_{l,\tau}+\beta_l\mathcal{M}^{\lambda}_{l,\tau}). \tag{15}$$

Sub-vector $\boldsymbol{b}_L$ is generated by the incident wave and $\boldsymbol{I}$ is the unit matrix. On the interfaces, pressure continuity and velocity equilibrium conditions have been assumed.

Solving Eq. (13) with direct linear equation numerical solvers such as LU decomposition and Gaussian elimination methods results in a memory cost in proportion to $O(N^2)$ and CPU time in proportion to $O(N^3)$. These disadvantages prevent the BEM based on the conventional algorithm from solving large-scale multi-domain acoustic problems. The FMBEM has been proved a very efficient fast solution method in solving large-scales acoustic problems. The approach to reduce the complexity of the matrix-vector computation using the FMM is discussed next.

3. Fast multipole boundary element method

3.1. Multipole expansion

To use the FMM to efficiently evaluate the matrix-vector multiplication with iterative solver, the source elements (here refer to the element of integration) of a field element (refers to element with the collocation point) are divided into two groups, named near group and far group, based on the tree structure. Contributions from the near group are calculated by direct method such as Gaussian quadrature, while contributions from the far group are evaluated by the FMM. Taking operator $\mathcal{S}^{\lambda}_{l,\tau}$ as an example, we will describe the computation of contributions from elements in a far group to a field element by the FMM in this section. Refer to Ref. [30] to get more details of the FMM algorithm. To simplify notations, the subscripts and superscript are omitted in $\mathcal{S}^{\lambda}_{l,\tau}$. Suppose $\boldsymbol{x}$ is the center of a field element and F_x is a set of all elements far from the element $\boldsymbol{x}$ in the sense of the tree structure. In light of Eq. (8) and using the fast multipole expansion of the kernel based on a plane wave expansion [31], contributions from all far enough elements to the field element are described by

$$\mathcal{S}q(\boldsymbol{y})=\frac{ik}{16\pi^2}\int_{\sigma_1}I(\hat{\boldsymbol{\sigma}},\boldsymbol{x},\boldsymbol{x}_c)T(\hat{\boldsymbol{\sigma}},\boldsymbol{x}_c,\boldsymbol{y}_c)\left(\int_{\Delta S_j\in F_{\boldsymbol{x}}}O(\hat{\boldsymbol{\sigma}},\boldsymbol{y}_c,\boldsymbol{y})q(\boldsymbol{y})dS(\boldsymbol{y})\right)d\sigma, \tag{16}$$

for $|\boldsymbol{x}-\boldsymbol{x}_c|<|\boldsymbol{y}-\boldsymbol{x}_c|$ and $|\boldsymbol{y}-\boldsymbol{y}_c|<|\boldsymbol{x}-\boldsymbol{y}_c|$, where $\boldsymbol{x}_c$ is an expansion point near $\boldsymbol{x}$ and $\boldsymbol{y}_c$ is that near $\boldsymbol{y}$. The translation, inner and outer functions in Eq. (16) are defined by

$$T(\hat{\boldsymbol{\sigma}},\boldsymbol{x}_c,\boldsymbol{y}_c)=\sum_{n=0}^{\infty}i^n(2n+1)h^{(1)}_n(ku)P_n(\hat{\boldsymbol{u}}\cdot\hat{\boldsymbol{\sigma}}), \tag{17}$$

$$I(\hat{\boldsymbol{\sigma}},x,\boldsymbol{x}_c)=e^{ik(\boldsymbol{x}-\boldsymbol{x}_c)\cdot\hat{\boldsymbol{\sigma}}}, \tag{18}$$

$$O(\hat{\boldsymbol{\sigma}},\boldsymbol{y}_c,\boldsymbol{y})=e^{ik(\boldsymbol{y}_c-\boldsymbol{y})\cdot\hat{\boldsymbol{\sigma}}}, \tag{19}$$

respectively, where $u=|\boldsymbol{x}_c-\boldsymbol{y}_c|$ and $\hat{\boldsymbol{u}}=(\boldsymbol{x}_c-\boldsymbol{y}_c)/u$, P_n is the nth order Legendre function, $\hat{\boldsymbol{\sigma}}=\hat{\boldsymbol{\sigma}}(\theta,\phi)=(\sin\theta\cos\phi,\sin\theta\sin\phi,\cos\theta)$ in which θ and ϕ are polar coordinates of point $\boldsymbol{\sigma}$ on the unit sphere σ_1.

The moment for a cell centered at $\boldsymbol{y}_c$, containing a set of elements Ω, are defined by

$$M(\hat{\boldsymbol{\sigma}},\boldsymbol{y}_c)=\sum_{\Delta S_j\in\Omega}\int_{\Delta S_j}e^{ik(\boldsymbol{y}_c-\boldsymbol{y})\cdot\hat{\boldsymbol{\sigma}}}q(\boldsymbol{y})dS(\boldsymbol{y}). \tag{20}$$

The moment of all cells is computed in the upward pass which traces the tree from the bottom to the top. Methods to compute the moment effectively are described in the Section 3.2. After obtaining the moments of cells, the local expansion for one cell centered at $\boldsymbol{x}_c$ is evaluated by collecting the moments of its well-separated cells and transferring the local expansions from its parent cell. Those well-separated cells of one cell are noted as the interaction list $\mathscr{L}$, the moment of all cells in a cell's interaction list is converted to the local expansion of the cell through

$$L(\hat{\boldsymbol{\sigma}},\boldsymbol{x}_c)=\sum_{\boldsymbol{y}_c\in\mathscr{L}}T(\hat{\boldsymbol{\sigma}},\boldsymbol{x}_c,\boldsymbol{y}_c)M(\hat{\boldsymbol{\sigma}},\boldsymbol{y}_c), \tag{21}$$

for $|\boldsymbol{x}-\boldsymbol{x}_c|<|\boldsymbol{y}-\boldsymbol{x}_c|$ and $|\boldsymbol{y}-\boldsymbol{y}_c|<|\boldsymbol{x}-\boldsymbol{y}_c|$, in which $\boldsymbol{x}$ is a field point located in the local cell whose center is $\boldsymbol{x}_c$, $\boldsymbol{y}$ is the source point located in one of the cells in the interaction list whose center is $\boldsymbol{y}_c$.

Generally, the number of sample points on a unit sphere σ_1 at a level depends on the cell size of the level. Due to the mismatch of sample points on the unit sphere, the moments and local expansions of cells at different levels cannot be passed to their child cells or parent cells directly. Interpolations become crucial to M2M and L2L translations because the overall accuracy and

computation complexity largely depend on these interpolations, especially for models with large tree structures. Jakob-Chien and Alpert [32] introduced an interpolation method with uniform resolution which is based on the FMM and fast Fourier transform (FFT). Sarvas [33] proposed an FFT method to perform the interpolations. Using the interpolation method, M2M and L2L are composed of two steps. First, in the upward pass the moments are temporarily shifted from the child level to the parent level. Conversely, in the downward pass the local expansions are temporarily shifted from the parent level to the child level. They are computed, respectively, by

$$\tilde{M}(\hat{\boldsymbol{\sigma}},\boldsymbol{y}_{c'}) = e^{ik(\boldsymbol{y}_{c'}-\boldsymbol{y}_c)\cdot\hat{\boldsymbol{\sigma}}} M(\hat{\boldsymbol{\sigma}},\boldsymbol{y}_c) \text{ for } \quad |\boldsymbol{y}-\boldsymbol{y}_{c'}| < |\boldsymbol{x}-\boldsymbol{y}_{c'}|, \tag{22}$$

$$\tilde{L}(\hat{\boldsymbol{\sigma}},\boldsymbol{x}_{c'}) = e^{ik(\boldsymbol{x}_c-\boldsymbol{x}_{c'})\cdot\hat{\boldsymbol{\sigma}}} L(\hat{\boldsymbol{\sigma}},\boldsymbol{x}_c) \quad \text{for } |\boldsymbol{x}-\boldsymbol{x}_{c'}| < |\boldsymbol{y}-\boldsymbol{x}_{c'}|. \tag{23}$$

Second, interpolations are performed over a unit spherical surface for the temporary moments and local expansions in the upward and downward passes, respectively, to reconstruct the final moments $M(\hat{\boldsymbol{\sigma}},\boldsymbol{y}_{c'})$ and local expansions $L(\hat{\boldsymbol{\sigma}},\boldsymbol{x}_{c'})$.

In the downward pass, when a leaf containing the point $\boldsymbol{x}$ is reached, the final evaluation of contributions from all far enough elements to the point $\boldsymbol{x}$ are computed by

$$\mathcal{S}q(\boldsymbol{y}) = \frac{ik}{16\pi^2}\int_{\sigma_1} I(\hat{\boldsymbol{\sigma}},\boldsymbol{x},\boldsymbol{x}_c) L(\hat{\boldsymbol{\sigma}},\boldsymbol{x}_c)\, d\sigma. \tag{24}$$

To reconstruct the contributions from all elements on the domain boundaries, direct numerical method is still needed to compute the contributions from elements contained in the adjacent cell.

The rest three operators defined in Eqs. (9)–(11)share the same M2M, M2L and L2L with the operator $\mathcal{S}$, except that moments of operators $\mathcal{D}$ and $\mathcal{H}$ should be computed by

$$M(\hat{\boldsymbol{\sigma}},\boldsymbol{x}_c) = \sum_{\Delta S_j \in \Omega}\int_{\Delta S_j} -ik\left(\frac{\partial \boldsymbol{y}}{\partial n(\boldsymbol{y})}\cdot\hat{\boldsymbol{\sigma}}\right) e^{ik(\boldsymbol{y}_c-\boldsymbol{y})\cdot\hat{\boldsymbol{\sigma}}}\varphi(\boldsymbol{y})\, dS(\boldsymbol{y}), \tag{25}$$

and final evaluations of operators $\mathcal{M}$ and $\mathcal{H}$ are

$$\mathcal{K}g(\boldsymbol{y}) = \frac{ik}{16\pi^2}\int_{\sigma_1} ik\left(\frac{\partial \boldsymbol{x}}{\partial n(\mathbf{x})}\cdot\hat{\boldsymbol{\sigma}}\right) I(\hat{\boldsymbol{\sigma}},\boldsymbol{x},\boldsymbol{x}_c) L(\hat{\boldsymbol{\sigma}},\boldsymbol{x}_c)\, d\sigma, \tag{26}$$

in which the symbol $\mathcal{K}$ represents either the operator $\mathcal{M}$ or $\mathcal{H}$, and correspondingly g represents q and φ.

Different from the usual single-domain FMBEM for acoustic problems in which either the sound pressure or velocity is given on each element, the multi-domain FMBEM considered in this paper needs to solve the two sets boundary quantities φ and q with coupled BIEs. In the multi-domain FMBEM, the FMM is actually used to compute

$$f(\boldsymbol{x}) = \boldsymbol{A}^{\lambda}_{l,\tau}\varphi_{\tau}(\boldsymbol{y}) + \boldsymbol{B}^{\lambda}_{l,\tau} q^{l}_{\tau}(\boldsymbol{y}), \tag{27}$$

for far enough points $\boldsymbol{x}$ and $\boldsymbol{y}$ in the sense of tree structure. Similar to the multipole expansions of the four operators introduced above, the moments of the multi-domain FMBEM in the lth domain are defined as

$$M(\hat{\boldsymbol{\sigma}},\boldsymbol{y}_c) = \sum_{\Delta S_j \in \Omega}\int_{\Delta S_j}\left[-q^{l}_{\tau}(\boldsymbol{y}) - ik_l\left(\frac{\partial \boldsymbol{y}}{\partial n(\boldsymbol{y})}\cdot\hat{\boldsymbol{\sigma}}\right)\varphi_{\tau}(\boldsymbol{y})\right] e^{ik_l(\boldsymbol{y}_c-\boldsymbol{y})\cdot\hat{\boldsymbol{\sigma}}}\, dS(\boldsymbol{y}), \tag{28}$$

and the final evaluation is computed by

$$f(\boldsymbol{x}) = \frac{ik}{16\pi^2}\int_{\sigma_1}\left(ik_l\beta_l\left(\frac{\partial \boldsymbol{x}}{\partial n(\mathbf{x})}\cdot\hat{\boldsymbol{\sigma}}\right)+1\right) I(\hat{\boldsymbol{\sigma}},\boldsymbol{x},\boldsymbol{x}_c) L(\hat{\boldsymbol{\sigma}},\boldsymbol{x}_c)\, d\sigma, \tag{29}$$

in which the local expansions $L(\hat{\boldsymbol{\sigma}},\boldsymbol{x}_c)$ are obtained from Eq. (21) based on the moments in Eq. (28).

In the diagonal form FMBEM, integration over the unit sphere in Eq. (29) is computed by p points Gaussian quadrature method in the θ direction and $2p$ points square quadrature in the ϕ direction [31]. To determine the number (p), the following empirical formulation is applied [34]:

$$p = kd + c_0\log(kd+\pi) \tag{30}$$

where d is the diameter of the cell on which integration are calculated, and c_0 is a number to determine the desired accuracy.

3.2. Effective moment computations

Suppose the number of sample points on the unit sphere in the θ direction is M, in the ϕ direction is P, and the number of elements contained in a cell is N. In light of Eq. (20), moments of a cell should be evaluated for all sample points on the unit sphere and all elements contained in the cell. That means for the cell, $M\times P\times N$ numerical evaluations of Eq. (20) need to be performed. For a large-scale model with large non-dimensional value ka, cost in computations of moments is very high. To reduce the cost of the computation, an analytical moment integration for the diagonal form acoustic FMBEM was proposed and had been demonstrated very efficient in solving acoustic problems [15].

In addition to the analytical moment, another method which can reduce the moments integrations by half is developed.This is based on the anti-symmetry of the moment kernel

$$e^{ik(\boldsymbol{y}_c-\boldsymbol{y})\cdot\hat{\boldsymbol{\sigma}}(\theta,\phi)} = e^{-ik(\boldsymbol{y}_c-\boldsymbol{y})\cdot\hat{\boldsymbol{\sigma}}(\pi-\theta,\pi+\phi)}. \tag{31}$$

For a constant element, its source strength $q(\boldsymbol{y})$ is a constant complex number. In order to use the anti-symmetry of the kernel to reduce the computation, the moment computation is divided into two steps. Moments for the upper hemisphere of the unit sphere for an element j are computed firstly,

$$M_j(\hat{\boldsymbol{\sigma}}(\theta,\phi),\boldsymbol{y}_c) = \int_{\Delta S_j} e^{ik(\boldsymbol{y}_c-\boldsymbol{y})\cdot\hat{\boldsymbol{\sigma}}}\, dS(\boldsymbol{y}) \quad \text{for } 0\le\theta\le\frac{\pi}{2}, \quad 0\le\phi\le 2\pi. \tag{32}$$

Using the fact in Eq. (31), moments for the lower hemisphere are calculated by

$$M_j(\hat{\boldsymbol{\sigma}}(\theta,\phi),\boldsymbol{y}_c) = M_j(\hat{\boldsymbol{\sigma}}(\pi-\theta,\pi+\phi),\boldsymbol{y}_c)^* \quad \text{for } \frac{\pi}{2}<\theta\le\pi, \quad 0\le\phi\le 2\pi, \tag{33}$$

in which * means complex conjugate. The final moments are given by

$$M(\hat{\boldsymbol{\sigma}}(\theta,\phi),\boldsymbol{y}_c) = \sum_{\Delta S_j\in\Omega} M_j(\hat{\boldsymbol{\sigma}}(\theta,\phi),\boldsymbol{y}_c) q(\boldsymbol{y}) \quad \text{for } 0<\theta\le\pi, \quad 0\le\phi\le 2\pi. \tag{34}$$

The above formulations are derived for operators $\mathcal{S}$ and $\mathcal{M}$. Operators $\mathcal{D}$ and $\mathcal{H}$ also share this characteristics. We name the characteristics as the anti-symmetry of moments in the diagonal FMBEM. For the linear element with the diagonal FMBEM, the computation of the moments can also be reduced by a factor of two using a similar method.

3.3. Multi-tree structure

The depth of a tree structure in the FMM has a significant influence on the efficiency of the multi-domain FMBEM. If the tree structure is too deep, the number of translations between levels will increase, and the numerical instability [35] for the diagonal FMMBEM, as used in this paper, may occur. In contrast, a small number of tree levels may increase adjacent interactions, thus pushing the portion of the direct numerical computation up which will affect the overall computational time. In multi-domain acoustic problems, due to different properties of the medium in the domains, the corresponding wavenumber varies from domains to domains. To tackle all these new challenges for the multi-domain FMBEM,

a multiple tree structure is adopted. This multiple tree structure assigns each domain a single tree that differs from the single tree structure for another domain and therefore complicates the implementation due to the different definitions of leaves on the interfaces.

In the iterative solution process, the matrix-vector multiplication of the multi-domain acoustic problems is computed domain by domain when using the multiple tree structure, and then the final productions of each domain are rearranged according to boundaries, as shown in Eq. (13). The multi-tree structure leads to each domain having two sets of coefficients, the moments and local expansions. Moments are calculated from the bottom to the top and stored for all cells in the upward pass. In the downward pass, local expansions are just translated between two adjacent levels, memory is not necessary to be allocated for all cells. A common memory block which can cover the largest local expansion for two adjacent levels is shared by cells for storing their local expansions in the downward pass. Since computation is performed domain by domain, therefore the memory for moments and common memory blocks for local expansions can be allocated according to the largest one among domains. If preconditioning is used, the sparse preconditioning matrices for each domain are usually saved for reusing to speed up the preconditioning inverse computation. However, this can result in large memory cost for the multi-domain FMBEM.

3.4. Preconditioner

Preconditioners for the FMBEM are crucial for its convergence and computing efficiency. Since the mismatch of cell definitions in adjacent domains, the usual block diagonal preconditioners based on the tree structure are not permissible. A preconditioner, named *pre-conditioner B* in Ref. [29] based on Eq. (11) therein, had been proved very effective for elastostatic inclusion problems. But as mentioned in [29], larger diagonal matrices need to be inverted which can be time-consuming if the number of elements on each inclusion is large. A compromising preconditioner based on the boundary block is proposed here, which can reduce the number of iteration for the GMRES solver as well as the time of the block diagonal matrix inverse. It can also reduce the memory size for storing the block diagonal coefficient matrices if it needs to reuse the coefficient matrices in the iteration.

The preconditioner is based on Eq. (13) while blocks are not based on the whole boundary of small domains. Blocks on a boundary are disjoint parts of the boundary which are divided by a certain method. One direct method to realize the boundary division is to use the tree structure generation algorithm while only leaves are referred, as shown in Fig. 2.

After grouping elements on each closed boundaryinto blocks, the discretized multi-domain BEM equations should be rearranged according to the blocks on boundaries. Suppose a special case with two boundaries (S_1 and S_2) and three domains (E_1, E_2 and E_3) and each boundary are divided into two blocks ($S_1 = S_{11} \cup S_{12}$, and $S_2 = S_{21} \cup S_{22}$), as shown in Fig. 3, the rearranged BEM equations can bedescribe as

$$\mathbf{M} = \begin{bmatrix}
\boldsymbol{A}^{11}_{1,11} & \rho_1\boldsymbol{B}^{11}_{1,11} & \boldsymbol{A}^{11}_{1,12} & \rho_1\boldsymbol{B}^{11}_{1,12} & \mathbf{0} & \mathbf{0} & \mathbf{0} & \mathbf{0} \\
\boldsymbol{A}^{11}_{2,11} & \boldsymbol{B}^{11}_{2,11} & \boldsymbol{A}^{11}_{2,12} & \boldsymbol{B}^{11}_{2,12} & \boldsymbol{A}^{11}_{2,21} & \rho_2\boldsymbol{B}^{11}_{2,21} & \boldsymbol{A}^{11}_{2,22} & \rho_2\boldsymbol{B}^{11}_{2,22} \\
\boldsymbol{A}^{12}_{1,11} & \rho_1\boldsymbol{B}^{12}_{1,11} & \boldsymbol{A}^{12}_{1,12} & \rho_1\boldsymbol{B}^{12}_{1,12} & \mathbf{0} & \mathbf{0} & \mathbf{0} & \mathbf{0} \\
\boldsymbol{A}^{12}_{2,11} & \boldsymbol{B}^{12}_{2,11} & \boldsymbol{A}^{12}_{2,12} & \boldsymbol{B}^{12}_{2,12} & \boldsymbol{A}^{12}_{2,21} & \rho_2\boldsymbol{B}^{12}_{2,21} & \boldsymbol{A}^{12}_{2,22} & \rho_2\boldsymbol{B}^{12}_{2,22} \\
\boldsymbol{A}^{21}_{2,11} & \boldsymbol{B}^{21}_{2,11} & \boldsymbol{A}^{21}_{2,12} & \boldsymbol{B}^{21}_{2,12} & \boldsymbol{A}^{21}_{2,21} & \rho_2\boldsymbol{B}^{21}_{2,21} & \boldsymbol{A}^{21}_{2,22} & \rho_2\boldsymbol{B}^{22}_{2,22} \\
\mathbf{0} & \mathbf{0} & \mathbf{0} & \mathbf{0} & \boldsymbol{A}^{21}_{3,21} & \boldsymbol{B}^{21}_{3,21} & \boldsymbol{A}^{21}_{3,22} & \boldsymbol{B}^{21}_{3,22} \\
\boldsymbol{A}^{22}_{2,11} & \boldsymbol{B}^{22}_{2,11} & \boldsymbol{A}^{22}_{2,12} & \boldsymbol{B}^{22}_{2,12} & \boldsymbol{A}^{22}_{2,21} & \rho_2\boldsymbol{B}^{22}_{2,21} & \boldsymbol{A}^{22}_{2,22} & \rho_2\boldsymbol{B}^{22}_{2,22} \\
\mathbf{0} & \mathbf{0} & \mathbf{0} & \mathbf{0} & \boldsymbol{A}^{22}_{3,21} & \boldsymbol{B}^{22}_{3,21} & \boldsymbol{A}^{22}_{3,22} & \boldsymbol{B}^{22}_{3,22}
\end{bmatrix}$$

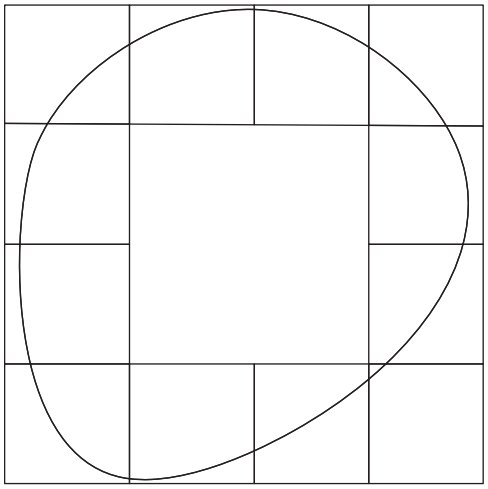

Fig. 2. An example of the blocks on the boundary for the preconditioner.

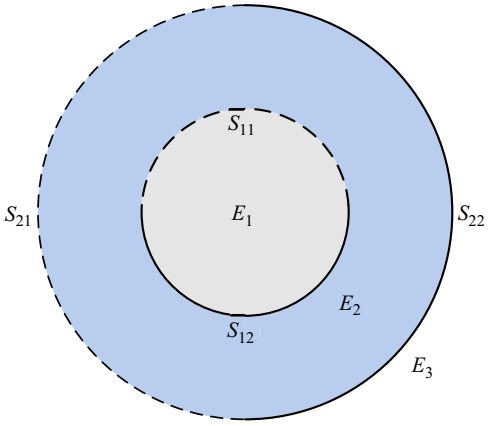

Fig. 3. A special case of boundary division.

$$\times \begin{bmatrix} \boldsymbol{\varphi}_{11} \\ \boldsymbol{q}_{11} \\ \boldsymbol{\varphi}_{12} \\ \boldsymbol{q}_{12} \\ \boldsymbol{\varphi}_{21} \\ \boldsymbol{q}_{21} \\ \boldsymbol{\varphi}_{22} \\ \boldsymbol{q}_{22} \end{bmatrix} = \begin{bmatrix} \mathbf{0} \\ \mathbf{0} \\ \mathbf{0} \\ \mathbf{0} \\ \mathbf{0} \\ \boldsymbol{b}_{21} \\ \mathbf{0} \\ \boldsymbol{b}_{22} \end{bmatrix}, \tag{35}$$

in which the double subscripts and superscripts "λn" means the nth block on the λth boundary. In this case, the following block diagonal matrix from the coefficient matrix in Eq. (35) is used as the preconditioner:

$$\mathbf{M} = \begin{bmatrix}
\boldsymbol{A}^{11}_{1,11} & \rho_1\boldsymbol{B}^{11}_{1,11} & \mathbf{0} & \mathbf{0} & \mathbf{0} & \mathbf{0} & \mathbf{0} & \mathbf{0} \\
\boldsymbol{A}^{11}_{2,11} & \boldsymbol{B}^{11}_{2,11} & \mathbf{0} & \mathbf{0} & \mathbf{0} & \mathbf{0} & \mathbf{0} & \mathbf{0} \\
\mathbf{0} & \mathbf{0} & \boldsymbol{A}^{12}_{1,12} & \rho_1\boldsymbol{B}^{12}_{1,12} & \mathbf{0} & \mathbf{0} & \mathbf{0} & \mathbf{0} \\
\mathbf{0} & \mathbf{0} & \boldsymbol{A}^{12}_{2,12} & \boldsymbol{B}^{12}_{2,12} & \mathbf{0} & \mathbf{0} & \mathbf{0} & \mathbf{0} \\
\mathbf{0} & \mathbf{0} & \mathbf{0} & \mathbf{0} & \boldsymbol{A}^{21}_{2,21} & \rho_2\boldsymbol{B}^{21}_{2,21} & \mathbf{0} & \mathbf{0} \\
\mathbf{0} & \mathbf{0} & \mathbf{0} & \mathbf{0} & \boldsymbol{A}^{21}_{3,21} & \boldsymbol{B}^{21}_{3,21} & \mathbf{0} & \mathbf{0} \\
\mathbf{0} & \mathbf{0} & \mathbf{0} & \mathbf{0} & \mathbf{0} & \mathbf{0} & \boldsymbol{A}^{22}_{2,22} & \rho_2\boldsymbol{B}^{22}_{2,22} \\
\mathbf{0} & \mathbf{0} & \mathbf{0} & \mathbf{0} & \mathbf{0} & \mathbf{0} & \boldsymbol{A}^{22}_{3,22} & \boldsymbol{B}^{22}_{3,22}
\end{bmatrix}. \tag{36}$$

The system of BEM equations in Eq. (35) is right preconditioned with the above block diagonal preconditioner as described

in Eq. (36). The diagonal sub-matrices in the preconditioner are obtained once and saved in memory for reusing in the subsequent iterations to save the CPU time.

4. Numerical examples

Numerical examples are presented in this section to demonstrate the accuracy and robustness of the FMBEM for multi-domain acoustic problems. The GMRES solver is used and the tolerance is set at 10^{-4}. All the simulations are done on a desktop PC with a 64-bit Intel® Core TM2 Duo CPU and 8 GB RAM, but only one core is used in the computation.

4.1. A sphere model

First, a penetrable sphere in an infinite domain and impinged by a plane wave with unit amplitude is investigated to verify the CHBIE formulations for the multi-domain acoustic problems. Radius of the sphere is $a=1$ m, as shown in Fig. 4. Sound speed and medium mass density in domain E_1 are $c_1=200$ m/s and $\overline{\rho}_1=2.01$ kg/m^3, in domain E_2 are $c_2=300$ m/s and $\overline{\rho}_2=3.01$ kg/m^3. The plane wave is traveling along $+z$-axis. In this case, analytical solution is available. Pressure in the exterior domain is

$$\varphi_2(\boldsymbol{x})=\sum_{n=0}^{\infty} i^n(2n+1)P_n(\cos\theta)[j_n(k_2|\boldsymbol{x}|)+a_n h_n(k_2|\boldsymbol{x}|)], \quad |\boldsymbol{x}|\geq a, \tag{37}$$

in which θ is the polar angle of point $\boldsymbol{x}$ in the spherical coordinates, and the series expansion coefficients a_n are defined by

$$a_n=\frac{\gamma j_n'(k_1a)j_n(k_2a)-j_n(k_1a)j_n'(k_2a)}{j_n(k_1a)h_n'(k_2a)-\gamma j_n'(k_1a)h_n(k_2a)}, \tag{38}$$

where j_n and h_n are first kind spherical Bessel and Henkel function of order n, respectively, and $\gamma=k_1/\rho_1k_2$. The non-dimensional value k_2a ranges from 2.0 to 10.0 by 500 steps, k_2 is the wavenumber in the E_2 domain. Corresponding elements in the model mesh increase from 3888 to 25,392. Boundary solutions are computed by the FMBEM with the CBIE and CHBIE, respectively. The sound pressures at the field point, (0, 2a, 0), are plotted in Fig. 5(a), which indicates that the BEM equations with the CBIE fail to give the correct result at the fictitious eigenfrequencies which correspond to $k_2a=n\pi$, $n=1,2,\ldots$. The relative errors of solutions given by the CBIE and CHBIE formulations with respect to the analytical solutions are plotted in Fig. 5(b). It shows that, away from the fictitious frequencies, solutions given by the CHBIE formulation are slightly worse than solutions given by the CBIE.

4.2. Two concentric spheres model

We next study the efficiency as well as the accuracy of the multi-domain FMBEM and the developed algorithm. The model used in this study is two concentric spheres immersed in an infinite domain E_3, as shown in Fig. 6, a cross section on the oyz plane. Radius of the inner sphere is $a=1$ m, the thickness of domain E_2 in the radius direction is $d=\gamma a$, where γ is set to be 0.25 in this study. The model is impinged upon by a plane wave traveling along $+z$-axis. In this case, sound speed and medium mass density in domain E_1 are $c_1=1500$ m/s and $\overline{\rho}_1=1000$ kg/m^3, in domain E_2 are $c_2=1324$ m/s and $\overline{\rho}_2=800$ kg/m^3, in domain E_3 are $c_3=1121$ m/s and $\overline{\rho}_3=791$ kg/m^3.

First, we set the frequency of the incident wave as a constant, $f_3=800$ Hz. Analytical solution is also available for this case.

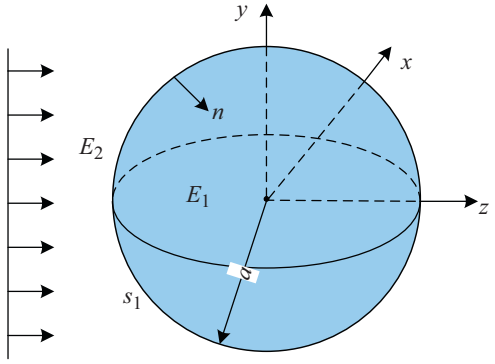

Fig. 4. A sphere model.

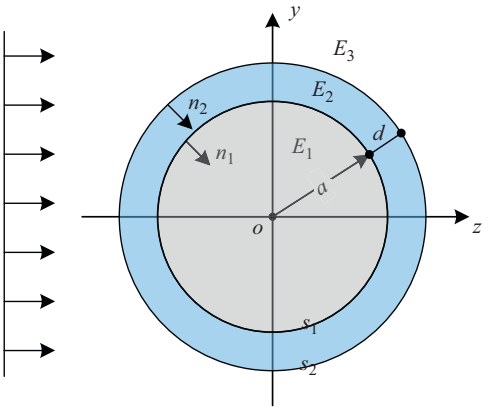

Fig. 6. Two concentric spheres.

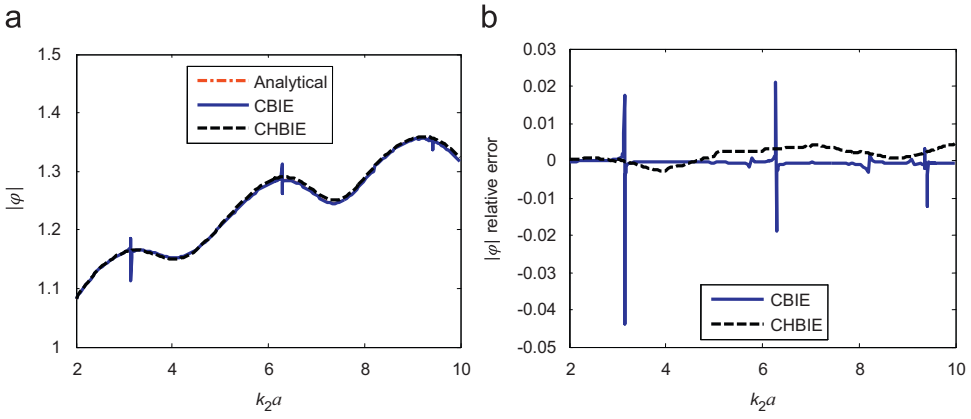

Fig. 5. Frequency sweep plot for a penetrable sphere scattering problem.

Theoretically, refining the discretization will make the solution converge to the analytical result. This fact is used to validate the accuracy of the multi-domain FMBEM. The total number of elements increases from 1068 to 29,496. Note that the dimension of corresponding BEM equations is twice as many as the total element number. The absolute relative error is defined in L2 norm, as

$$Error = \frac{\|(\varphi_{num}-\varphi_{ana})+(q_{num}-q_{ana})\|}{\|\varphi_{ana}+q_{ana}\|}, \tag{39}$$

in which φ_{num} and q_{num} are the corresponding numerical results solved with the FMBEM or the conventional BEM based on the Burton–Miller formulation, φ_{ana} and q_{ana} are analytical solutions. The error curve is plotted in Fig. 7. It shows that solutions obtained by the FMBEM and BEM agree very well with each other. The error goes down with increasing the number of elements and converges, which demonstrates the accuracy of the multi-domain FMBEM. In the simulations, the iterative number increases from 36 to 46 and reaches the constant number 46 for the last three steps in this case. The CPU times and the memory usages are plotted in Figs. 8 and 9 which do demonstrate advantages of the multi-domain FMBEM in CPU time cost and memory allocation. In Fig. 9, memory requirements for the FMBEM include the memory assigned for the direct coefficients storage, and the dash line means estimated memory used in the conventional BEM.

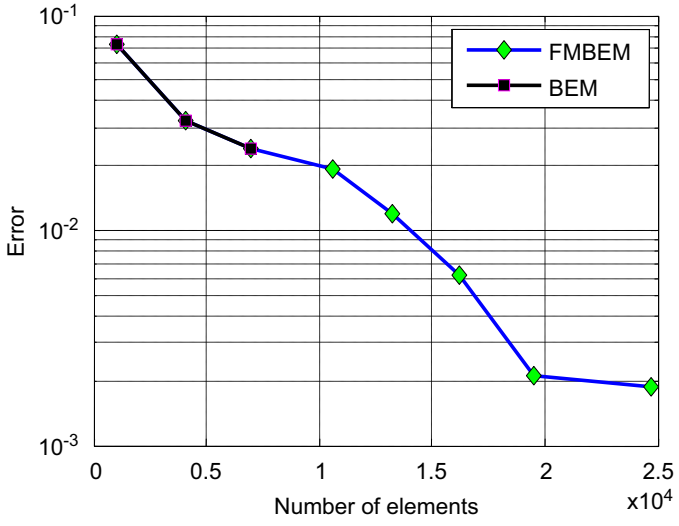

Fig. 7. Relative errors of solutions given by the FMBEM and conventional BEM.

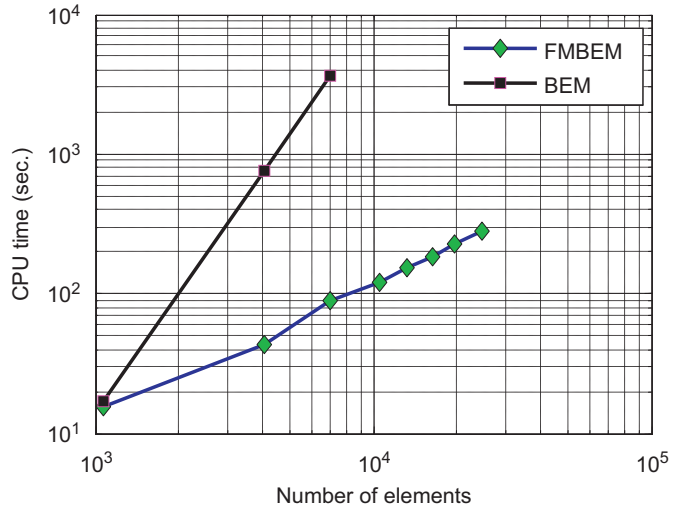

Fig. 8. CPU times used by the FMBEM and conventional BEM.

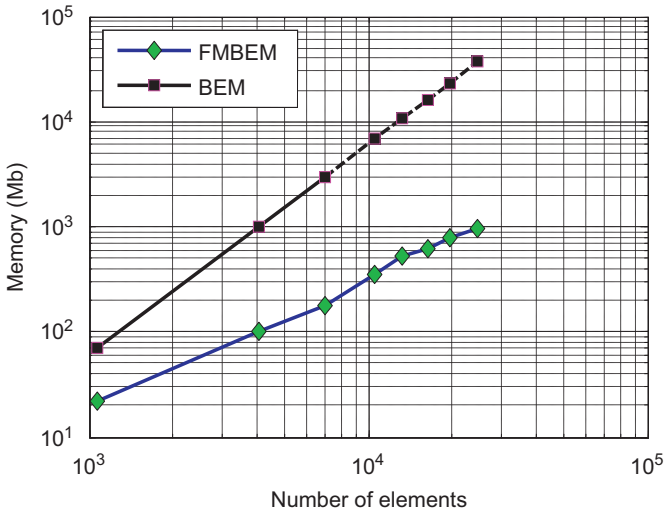

Fig. 9. Memory used by the FMBEM and conventional BEM.

Table 1
Element numbers, iteration numbers and errors for the two concentric spheres scattering at different frequencies.

Frequency (Hz)	Element no.		Preconditioning			Error
	Inner	Outer	Case 1	Case 2	Case 3	
200	1728	2700	30	18	17	2.150E−03
400	4800	6438	44	30	27	1.788E−03
600	9408	11,532	60	43	36	1.326E−03
800	15,552	19,200	85	57	47	1.192E−03
1000	24,300	30,000	103	87	74	9.060E−03
1200	36,300	43,200	152	99	85	7.265E−03
1400	44,652	55,488	155	99	81	6.500E−03
1600	58,800	86,700	255	137	109	1.900E−03
1800	76,800	120,000	279	194	152	1.503E−03

To validate the accuracy and demonstrate the efficiency of the multi-domain FMBEM for a wide range of frequencies, another simulation is performed for the two concentric spheres model. The incident wave frequency increases from 200 Hz to 1800 Hz with 9 steps. The numbers of total element varying with the increasing frequency are given in Table 1, and the corresponding errors, defined in Eq. (39), of the FMBEM solutions are also listed therein, which further demonstrates the accuracy of the developed multi-domain FMBEM. The perconditioner's performance is explored in this study. First, no preconditioned GMRES solver is used to compute the results at the 9 steps. Then the right preconditioned GMRES with different configurations, in which the maximum elements (*Bmaxl*) allowed in the boundary block division using the tree generation algorithm are set to 20 and 60, respectively, are employed to solve the results at the 9 steps. Iteration numbers used in those different solver configurations are included in Table 1, in which case 1, 2 and 3 correspond to no preconditioning, *Bmaxl* is 20, and 60. Obviously, significant achievement is made in convergence rates in the iterative solution by using the preconditioner in Eq. (36), which is based on the BEM equations in Eq. (35). For some steps, no big differences in the iteration number between cases 1 and 2. That is because block structures generated by the two *Bmaxl*s are slightly different due to the model's geometry. However, without preconditioner the iteration number grows up quickly with respective to the increasing frequency. That high growth rate with respect to frequency does not show up in the single domain FMBEM. So that,

preconditioner is even more crucial to the multi-domain FMBEM. Fig. 10 is a plot of CPU times used for the calculations with and without preconditioner. Memory requirements for preconditioner with different *Bmaxl*s are plotted in Fig. 11. The bigger the *Bmaxl* is the larger the memory needed as indicated in Fig. 11. If the double precision format is used, the size of memory for the preconditioner is bounded by $6.1035\text{E}-5 \times Bmaxl \times N\text{Mb}$, which assumes that all the blocks have *Bmaxl* elements. As indicated in Fig. 11, the memory size for the preconditioner is $O(Bmaxl\ N \log N)$.

4.3. Scattering from a cubic box nested with multiple spheres

Amore complex multi-domain scattering model is investigated next. The model is a cubic box in a $5\text{ m} \times 5\text{ m} \times 5\text{ m}$ domain containing 27 uniformly distributed spheres whose radius is 0.5 m, and immersed in an infinite domain, as shown in Fig. 12. Spherical domains have the same sound speed, 1190 m/s, and the same mass density, 791 kg/m^3. The cubic box domain and the out most domain share the same sound speed and mass density of the domains E_2 and E_3 in the previous case, respectively. The incident plane wave with unit magnitude is traveling along $+z$-axis with

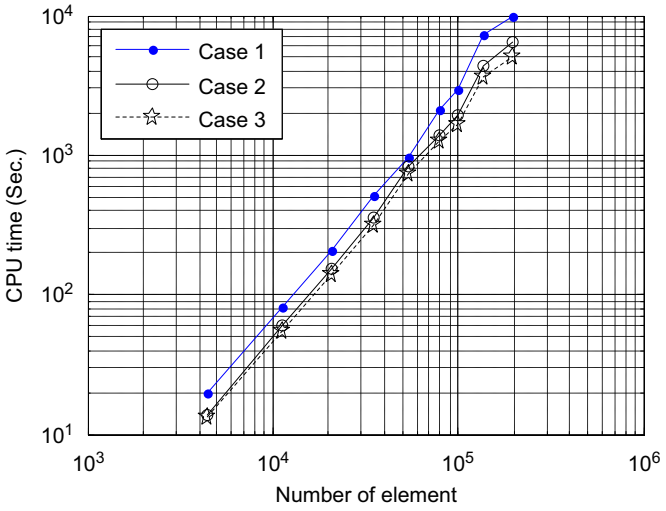

Fig. 10. CPU times used for solutions with and without preconditioner.

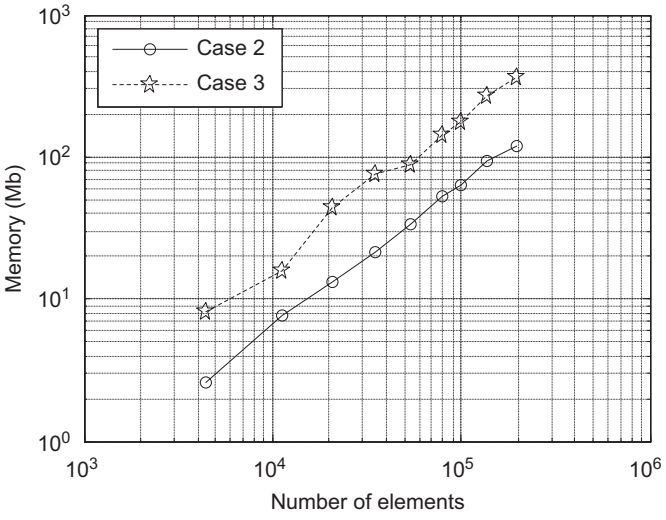

Fig. 11. Memory requirements for preconditioner with different *Bmaxl*s.

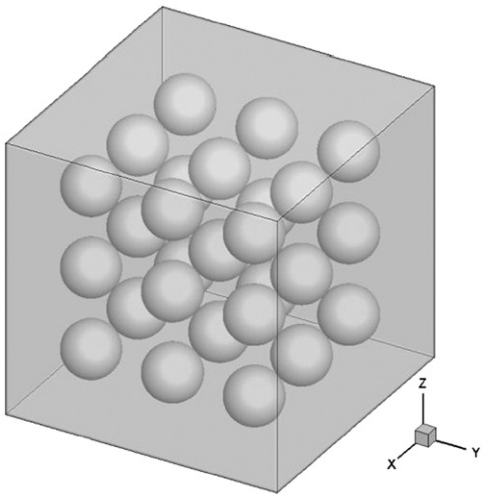

Fig. 12. A cubic box nested with multiple spheres.

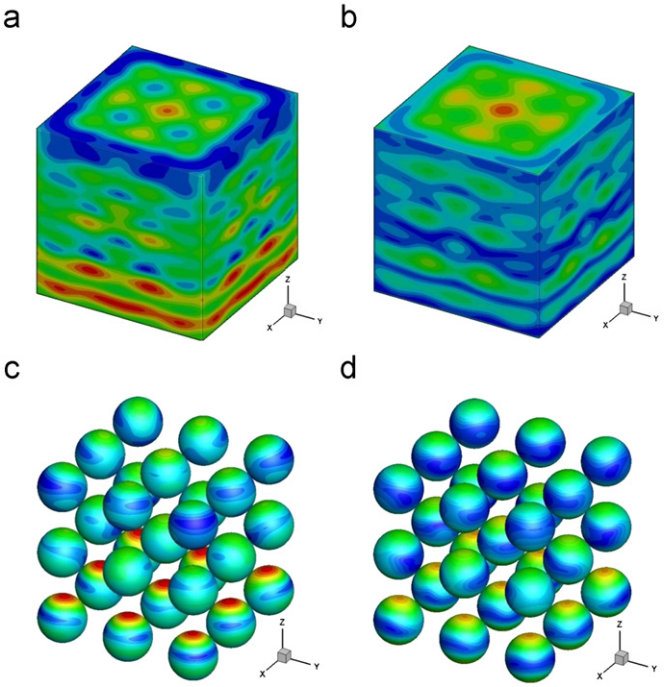

Fig. 13. Boundary solutions: (a) and (c) are $|\varphi|$ solutions of the cubic box's and multiple spheres boundaries, (b) and (d) are $|q|$ solutions of the cubic box's and multiple spheres boundaries.

the frequency of 1000 Hz. The maximum element number allowed in the boundary block is set to 80. The maximum element number allowed in a leaf in domain trees is set to 40. The tolerance for convergence of the solution is set to 10^{-3} in this case. Each sphere is meshed with 7500 triangular elements, and the cubic box is meshed with 120,000 triangular elements. Right preconditioned GMRES is used in the computation. The total number of elements used in this model is 322,500 (and the dimension of the BEM equations is $2 \times 322{,}500$). The number of iteration used and CPU time spent in this case are 137 times and 10,230 s, respectively, which further demonstrate the potential of the developed multi-domain FMBEM in solutions of large-scale multi-domain acoustic problems. It is worth noting that the CPU time used in this case is 12,332 s if the anti-symmetry of moment is not applied. The boundary solutions and computed field pressure on a surface are plotted in Figs. 13 and 14.

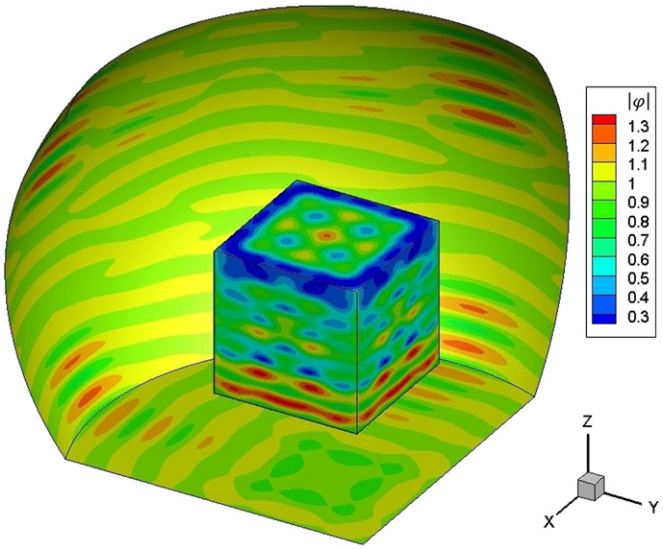

Fig. 14. Computed pressure on a field surface and the cubic box boundary.

5. Conclusion

In this paper, a fast multipole boundary element method (FMBEM) for 3D multi-domain acoustic problems is developed, which can have a broad range of applications, such as in the characterization of sound absorbing materials, underwater acoustics and biomedical applications. The multi-domain FMBEM is based on the Burton–Miller BIE formulation. It can give unique solutions at the fictitious eigenfrequencies, which is demonstrated by the frequency sweep analysis for a single sphere scattering model. Since the wavenumber usually varies among domains, multi-tree structure is employed in the multi-domain FMBEM. To overcome the mismatch of the cell definition in domains, the BEM equations are reformulated according to boundaries, which allows the adoption of the boundary block diagonal preconditioner. The boundary block diagonal preconditioner assembles the coefficients of submatrices in blocks as block diagonal matrices to approximate the BEM coefficient matrix. The larger the block sizes are, the closer the assembled matrix approximates to the BEM coefficient matrix and the larger memory the preconditioner takes. If domains have the same geometry and same material properties, as the case in Section 4.3, those domains can share the same preconditioners. This special case can save the memory for storing the preconditioners. However, this technique is not applied in the current work with the intent to leave the developed multi-domain FMBEM code as general as possible so that it can be applied to solve a broader range of multi-domain acoustic problems.

Although the boundary block preconditioner devised for the multi-domain FMBEM turns out to be very efficient in reducing the iteration number, as indicated by the two concentric sphere scattering example, preconditioning for the multi-domain acoustic FMBEM still remains as an subject of study. Sometime the block size needs to be set as a larger number to get a good convergence rate in the iterative solution. In addition to the high preconditioning cost, the multi-tree structure also leads to larger memory requirement and high CPU time cost. These challenges make the multi-domain FMBEM not possible now to solve the large-scale acoustic problems as large as the single-domain FMBEM has dealt with. Additional improvements are needed. The multi-domain FMBEM developed in this paper can also be applied to solve multi-layered acoustic problems. For multi-layered problems, the BEM equations are similar to Eq. (13) except that each layer just has two boundaries which may lead to a sparse coefficient matrix.

Acknowledgment

The work is supported by grant 11074170 of the National Natural Science Foundation of China and grant MSVMS201105 of the National State Key Laboratory Foundation.

References

[1] Rokhlin V. Rapid solution of integral equations of classical potential theory. J Comput Phys 1985;60(2):187–207.
[2] Greengard L, Rokhlin V. A fast algorithm for particle simulations. J Comput Phys 1987;73(2):325–48.
[3] Greengard L. The rapid evaluation of potential fields in particle systems. London: The MIT Press; 1988.
[4] Saad Y, Schultz MH. GMRES: a generalized minimal residual algorithm for solving nonsymmetric linear systems. SIAM J Sci Stat Comput 1986;7(3):856–69.
[5] Sonneveld P. GGS: a fast Lanczos-type solver for nonsymmetric linear systems. SIAM J Sci Stat Comput 1989;10:36–52.
[6] Sakuma T, Yasuda Y. Fast multipole boundary element method for large-scale steady-state sound field analysis. Part I: Setup and validation. Acta Acust United Ac 2002;88(4):513–25.
[7] Yasuda Y, Sakuma T. Fast multipole boundary element method for large-scale steady-state sound field analysis. Part II: Examination of numerical items. Acta Acustica (Stuttgart) 2003;89(1):28–38.
[8] Gumerov NA, Duraiswami R. Computation of scattering from clusters of spheres using the fast multipole method. J Acoust Soc Am 2005;117(41):1744–61.
[9] Fischer M, Gaul L. Application of the fast multipole bem for structural-acoustic simulations. J Comput Acoust 2005;13(1):87–98.
[10] Gaul L, Fischer M. Large-scale simulations of acoustic-structure interaction using the fast multipole BEM. Z Angew Math Mech 2006;86(1):4–17.
[11] Brunner D, Junge M, Gaul L. Simulation of elastic scattering with a coupled FMBE–FE approach. Crete 2009:137–48.
[12] Shen L, Liu YJ. An adaptive fast multipole boundary element method for three-dimensional acoustic wave problems based on the Burton–Miller formulation. Comput Mech 2007;40(3):461–72.
[13] Bapat MS, Shen L, Liu YJ. Adaptive fast multipole boundary element method for three-dimensional half-space acoustic wave problems. Eng Anal Bound Elem 2009;33(8-9):1113–23.
[14] Bapat MS, Liu YJ. A new adaptive algorithm for the fast multipole boundary element method. Comput Model Eng Sci 2010;58(2):161–83.
[15] Wu HJ, Liu YJ, Jiang WK. Analytical integration of the moments in the diagonal form fast multipole boundary element method for 3-D acoustic wave problems. Eng Anal Bound Elem 2012;36:248–54.
[16] Darve E, Havé P. A fast multipole method for Maxwell equations stable at all frequencies. Philos Trans R Soc A: Math Phys Eng Sci 2004;362(1816):603–28.
[17] Cheng H, Crutchfield WY, Gimbutas Z, Greengard LF, Ethridge JF, Huang J, et al. A wideband fast multipole method for the Helmholtz equation in three dimensions. J Comput Phys 2006;216(1):300–25.
[18] Gumerov NA, Duraiswami RA. A broadband fast multipole accelerated boundary element method for the three dimensional Helmholtz equation. J Acoust Soc Am 2009;125(1):191–205.
[19] Nishimura N. Fast multipole accelerated boundary integral equation methods. Appl Mech Rev 2002;55(4):299–324.
[20] Liu YJ. Fast multipole boundary element method: theory and applications in engineering. Cambridge University Press; 2009.
[21] Cheng CYR, Seybert AF, Wu TW. A multidomain boundary element solution for silencer and muffler performance prediction. J Sound Vib 1991;151(1):119–29.
[22] Sarradj E. Multi-domain boundary element method for sound fields in and around porous absorbers. Acta Acustica (Stuttgart) 2003;89(1):21–7.
[23] Seydou F, Duraiswami R, Seppanen T. Three dimensional acoustic scattering from an M multilayered domain via an integral equation approach. In: AP–S International Symposion (Digest), Columbus, 04, vol.1. IEEE Antennas and Propagation Society; 2003. p. 669–72.
[24] Chen S, Liu YJ. A unified boundary element method for the analysis of sound and shell-like structure interactions. I. Formulation and verification. J Acoust Soc Am 1999;106(31):1247–54.
[25] Chen K, Harris PJ. Efficient preconditioners for iterative solution of the boundary element equations for the three-dimensional Helmholtz equation. Appl Numer Math 2001;36(4):475–89.
[26] Guillaume P, Huard A, Le Calvez C. A block constant approximate inverse for preconditioning large linear systems. SIAM J Matrix Anal Appl 2003;24(3):822–51.

[27] Wang H, Yao Z, Wang P. On the preconditioners for fast multipole boundary element methods for 2D multi-domain elastostatics. Eng Anal Bound Elem 2005;29(7):673–88.
[28] Burton AJ, Miller GF. The application of integral equation methods to the numerical solution of some exterior boundary-value problems. Proc R Soc London. Ser A Math Phys Sci 1971;323(1553):201–10.
[29] Liu YJ. A fast multipole boundary element method for 2D multi-domain elastostatic problems based on a dual BIE formulation. Comput Mech 2008;42(5): 761–73.
[30] Liu YJ, Nishimura N. The fast multipole boundary element method for potential problems: a tutorial. Eng Anal Bound Elem 2006;30(5):371–81.
[31] Rahola J. Diagonal forms of the translation operators in the fast multipole algorithm for scattering problems. BIT Numer Math 1996;36(2):333–58.
[32] Jakob-Chien R, Alpert BK. A fast spherical filter with uniform resolution. J Comput Phys 1997;136(2):580–4.
[33] Sarvas J. Performing interpolation and anterpolation entirely by fast fourier transform in the 3-D multilevel fast multipole algorithm. SIAM J Numer Anal 2003;41(6):2180–96.
[34] Coifman R, Rokhlin V, Wandzura S. The fast multipole method for the wave equation: a pedestrian prescription. Antennas Propag Mag IEEE 1993;35(3):7–12.
[35] Nilsson M. Stability of the high frequency fast multipole method for Helmholtz' equation in three dimensions. BIT Numer Math 2004;44(4):773–91.